Real-time Visualization of High-Dynamic-Range Infrared Images based on Human Perception Characteristics

Noise Removal, Image Detail Enhancement and Time Consistency

Frederic Garcia, Cedric Schockaert and Bruno Mirbach
PTU Optical, IEE S.A., 11, rue Edmond Reuter, Contern, Luxembourg

Keywords: Detail Enhancement, Contrast Enhancement, Noise Removal, High-Dynamic-Range, Infrared Images, Human Perception, Time Filtering.

Abstract: This paper presents an image detail enhancement and noise removal method that accounts for the limitations on human's perception to effectively visualize high-dynamic-range (HDR) infrared (IR) images. In order to represent real world scenes, IR images use to be represented by a HDR that generally exceeds the working range of common display devices (8 bits). Therefore, an effective HDR compression without loosing the perceptibility of details is needed. We herein propose a practical approach to effectively map raw IR images to 8 bit data representation. To do so, we propose an image processing pipeline based on two main steps. First, the raw IR image is split into base and detail image components using the guided filter (GF). The base image corresponds to the resulting edge-preserving smoothed image. The detail image results from the difference between the raw and base images, which is further masked using the linear coefficients of the GF, an indicator of the spatial detail. Then, we filter the working range of the HDR along time to avoid global brightness fluctuations in the final 8 bit data representation, which results from combining both detail and base image components using a local adaptive gamma correction (LAGC). The last has been designed according to the human vision characteristics. The experimental evaluation shows that the proposed approach significantly enhances image details in addition to improving the contrast of the entire image. Finally, the high performance of the proposed approach makes it suitable for real word applications.

1 INTRODUCTION

In contrast to common cameras where images are formed using visible light (450-750 nm), IR cameras operate using IR radiations (wavelengths as long as 14 μm). Therefore, the variation of the measuring range might be considerable in real world scenarios, *e.g.,* thermal measures from the sky against those from the engine of a driving car. This implies the use of high-precision analog to digital (ADC) data converters which entails to use either 12 or 14 bits for data representation. On the other side, display devices are intended to display 8 bit data, requiring IR images to be compressed for visualization, which may yield to the loss of significant details.

The literature presents a vast number of useful image processing techniques to increase the image contrast, enhance image details and/or reduce the amount of noise. Although most of these techniques are intended for 8 bit still images, they can be adapted and/or combined to address the enhancement of IR image details whilst compressing its HDR into a proper range for display. Indeed, variations of gamma correction (GC) and histogram equalization (HE) approaches have been widely used to fit the raw data into a 8 bit data representation with an increase of the global contrast. Silverman (Silverman, 1993) enhanced the contrast in dominating temperature ranges of the scene and addressed several issues inherent in the traditional HE (Pizer et al., 1987), such as noise amplification within uniform areas. Similarly, Vickers (Vickers, 1996) extended the traditional HE with the known Plateau-HE, where the dominating intensities of the histogram were clipped and thus, leading to a reduction of the amplification of noise within uniform areas. To better enhance local details in the image with a better robustness against noise, local methods such as Adaptive HE (AHE) (Pizer et al., 1987) or Contrast Limited AHE (CLAHE) (Zuiderveld, 1994) might be considered. Those methods are based on the computation and processing of a local histogram. A spatial interpolation is performed in order to avoid

Garcia F., Schockaert C. and Mirbach B..
Real-time Visualization of High-Dynamic-Range Infrared Images based on Human Perception Characteristics - Noise Removal, Image Detail Enhancement and Time Consistency.
DOI: 10.5220/0005309501440152
In *Proceedings of the 10th International Conference on Computer Vision Theory and Applications* (VISAPP-2015), pages 144-152
ISBN: 978-989-758-089-5

visible artefacts after the local processing. However, those methods are usually computationally expensive due to their high level of complexity. In (Kim et al., 2001), a method called Partially Overlapped Sub-Block HE was proposed to highlight the detail contrast for a lower computation time. However, small details are highly attenuated or removed. To overcome this issue, Liang et al (Liang et al., 2012) proposed to locally apply a double local plateau histogram in order to enhance the background while preserving the details. In order to significantly reduce the noise without attenuating or removing image details, Durand and Dorsey (Durand and Dorsey, 2002) suggested the use of an edge-preserving filter to split the IR image into base and detail image components and process them separately. More recent, many efforts have been done on the processing of each image component as well as on their combination.

Inspired by the idea of splitting the raw IR image in base and detail image components suggested by Durand and Dorsey (Durand and Dorsey, 2002), we herein propose a new pipeline to efficiently enhance important image details whilst suppressing noise and increasing the global image contrast, satisfying the human visual perception.

The remainder of the paper is organized as follows: Section 2 covers the literature review on recent detail enhancement and visualization techniques for IR images. In Section 3 we present the proposed approach for real-time visualization of HDR IR images. Section 4 presents the evaluation of the proposed approach in which real IR scenes have been considered. A comparison against the most recent DDE-based filters is also provided. Finally, concluding remarks and future work directions are given in Section 5.

2 RELATED WORK

Recent IR image visualization approaches are strongly related to the enhancement of the details in the resulting 8 bit image representation. Glush et al. (Glushko and Salvaggio, 2007) limited the noise amplification by the so-called unsharp masking, a technique that defines a detail map to classify noise and detail pixels depending on the intensity of the detail. An alternative approach is the Balanced CLAHE and Contrast Enhancement (BCLAHE-CE), an extension of CLAHE in combination with contrast enhancement and HDR compression that was proposed in (Branchitta et al., 2008). As suggested by Durand and Dorsey (Durand and Dorsey, 2002), bilateral filter (BF) has been widely used to define a detail map. An example is the Filter and Dynamic Range Partitioning (BF&DRP) presented in (Branchitta et al., 2009). However, it is known that BF suffers from gradient reversal artefacts along edges, which might be visible in the resulting 8 bit image. Zuo et al. (Zuo et al., 2011) addressed the gradient reversal artefact on their BF-based Digital Detail Enhancement (BF&DDE) filter by applying a Gaussian low pass filter on the resulting base image component. In addition, the BF coefficients were used to enhance the image details while keeping a low level of noise. In (Karali et al., 2010), the authors proposed a technique that classifies objects and background *e.g.,* sea and sky. Therefore, only objects were enhanced. A Fourier analysis was performed to define the base image, medium detail map and fine detail map, which was enhanced by respective multiplicative gain allowing a reduction of the halo on warm objects. More recently, He et al. (He et al., 2013) presented a new edge preserving filter, the so-called guided filter (GF). As suggested by the authors, the GF might be also considered to define the detail map, replacing the BF. Indeed, in contrast to the BF, GF does not suffer from the edge artefact and its processing time is significantly smaller. Liu et al. (Liu and Zhao, 2014) updated their previous work (Zuo et al., 2011) by using GF instead of BF. As expected, the GF&DDE performance significantly increased while presenting very close results. However, the above presented approaches are intended for static IR images, which produce a non desired variation of the background intensity values when applied to a video sequence.

In the following, we present the so-called Temporal DDE (TDDE) filter which, in addition to enhance and preserve image details with an effective HDR compression, it addresses the temporal constraint to avoid global brightness fluctuations along the resulting 8 bit image sequence. Similarly to (Liu and Zhao, 2014), the TDDE filter also uses the GF to define the detail map. However, it differs from alternative DDE-based filters in the way to combine the resulting base and detail image components. Indeed, no data rearrangement is needed in the combination process. Inspired from (Liu et al., 2012), the 8 bit conversion uses a local adaptive gamma correction (LAGC) based on the Weber's law. Therefore, the TDDE filter is more suited to the human visual perception.

3 PROPOSED APPROACH

Fig. 1 presents the flow diagram of the proposed TDDE filter in which, following the advise of Durand and Dorsey (Durand and Dorsey, 2002) we split the raw IR image **I** into base **B** and detail **D** image com-

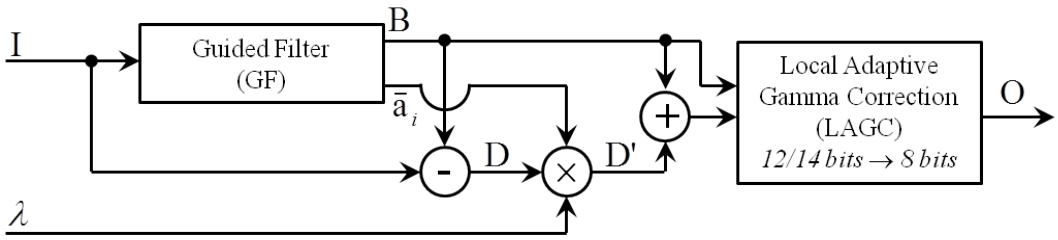

Figure 1: Flow diagram of the proposed TDDE filter.

ponents. This in turn, allows us to independently enhance and preserve image details whilst compressing the HDR.

3.1 Base Image Component

Similarly to (Zuo et al., 2011; He et al., 2013; Liu and Zhao, 2014), we also rely on the advise of He et al. (He et al., 2013) when choosing the GF to split **I** into base **B** and detail **D** image components. GF presents better behaviour near edges than BF with a major advantage of being a fast and non-approximate linear time algorithm, regardless of the kernel size and the intensity range. In addition, it does not suffer from the gradient reversal artefacts of BF (Zuo et al., 2011; He et al., 2013). The **B** image component is then the resulting edge-preserving smoothed image, a linear transform of **I** in a window w_k centred at pixel k, *i.e.,*

$$\mathbf{B}_i = \bar{\mathbf{a}}_i \mathbf{I}_i + \bar{\mathbf{b}}_i, \quad \forall i \in w_k, \tag{1}$$

where

$$\bar{\mathbf{a}}_i = \frac{1}{|w|} \sum_{k \in w_i} \mathbf{a}_k, \text{ with } \mathbf{a}_k = \frac{\frac{1}{|w|}\sum_{i \in w_k} \mathbf{I}_i^2 - \bar{\mathbf{I}}_k^2}{\sigma_k^2 + \varepsilon}, \tag{2}$$

$$\bar{\mathbf{b}}_i = \frac{1}{|w|} \sum_{k \in w_i} \bar{\mathbf{I}}_k - \mathbf{a}_k \bar{\mathbf{I}}_k, \tag{3}$$

are linear coefficients assumed to be constant in w_k. σ_k^2 is the variance of **I** in w_k, $|w|$ is the number of pixels in w_k, ε is a regularization parameter penalizing large $\mathbf{a}_k$, and $\bar{\mathbf{I}}_k = \frac{1}{|w|}\sum_{i \in w_k} \mathbf{I}_i$ is the mean of **I** in w_k. The selection of the w_k size might be done accordingly to the minimum size of the details to be preserved in **I**. Herein, we choose a small w_k size (3×3) in order to preserve and enhance fine details such as trees' leaves. The smoothing level is given by the ε parameter. That is, if ε is setted too small, *e.g.,* 10, not only image details are preserved but also noise and tiny structures in the image. Therefore, a good compromise is to set a small window size and a large ε value. By doing so, details along strong edges will be preserved whereas uniform regions will be smoothed. Fig. 3 presents different **B** images illustrating the behaviour of the GF depending on the chosen window size and ε parameters. We note that bigger ε values will dramatically increase the smoothing effect when combined with larger w_k sizes (see Fig. 3(e) and Fig. 3(f)). The input raw image **I** shown in Fig. 2 has been considered as a test case.

Figure 2: Raw input image **I** used as a test case.

3.2 Detail Image Component

In general, the detail image component **D** results from the difference between the input raw image **I** and the filtered **B** image, *i.e.,* $\mathbf{D} = \mathbf{I} - \mathbf{B}$. In Fig. 4, we present the detail images **D** that result from the difference between **I** in Fig. 2 and each **B** image component in Fig. 3. As above-mentioned, not only tiny details but also noise is present in **D** when setting ε too small (see Fig. 4(a)). Instead, noise can be significantly reduced by setting ε big enough (see Fig. 4(c)). But, this in turn will suppress desired details in **D**. Therefore, a tradeoff between noise removal and detail preserve needs to be chosen, even though retained noise may be identified as details and thus enhanced by mistake in the resulting 8 bit image.

According to the human perception, noise within smooth image regions can be easily perceive by the observer as spurious or texture whereas it is almost imperceptible along sharp edges. Taking that into account, we propose to mask the noise depending on the spatial detail. To that end, we have considered the linear coefficient $\bar{\mathbf{a}}_i$ that results from the GF. As can be observed in Fig. 6, $\bar{\mathbf{a}}_i$ clearly reflects the spatial detail of the image. Thus, we can significantly

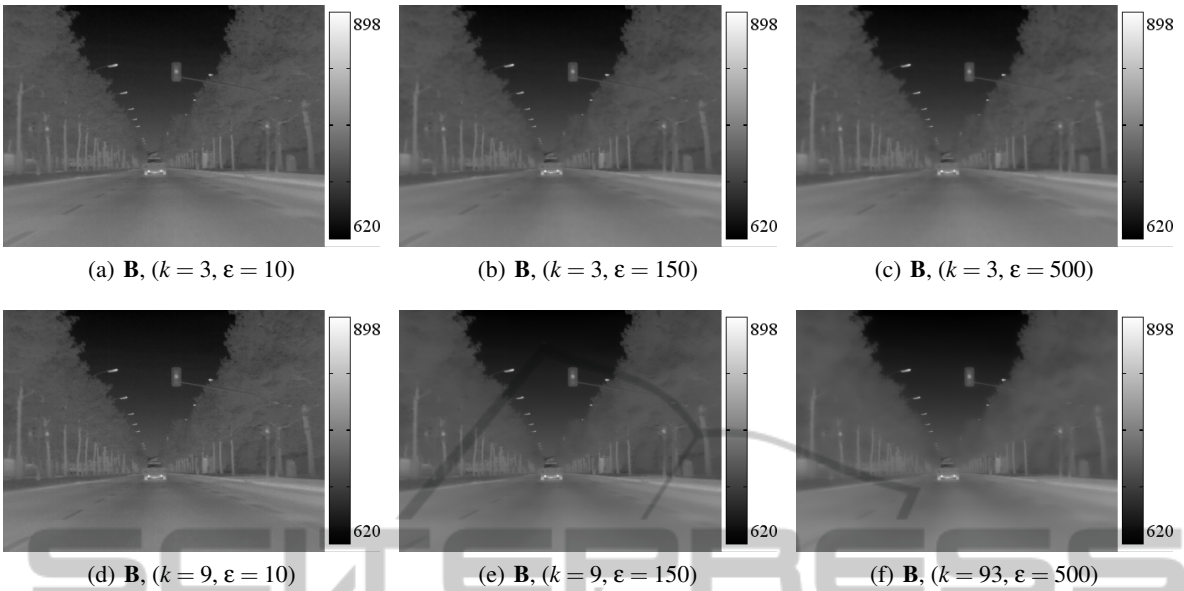

(a) **B**, ($k = 3$, $\varepsilon = 10$) (b) **B**, ($k = 3$, $\varepsilon = 150$) (c) **B**, ($k = 3$, $\varepsilon = 500$)

(d) **B**, ($k = 9$, $\varepsilon = 10$) (e) **B**, ($k = 9$, $\varepsilon = 150$) (f) **B**, ($k = 93$, $\varepsilon = 500$)

Figure 3: **B** images illustrating the behaviour of the GF depending on the window w_k size and the ε parameter.

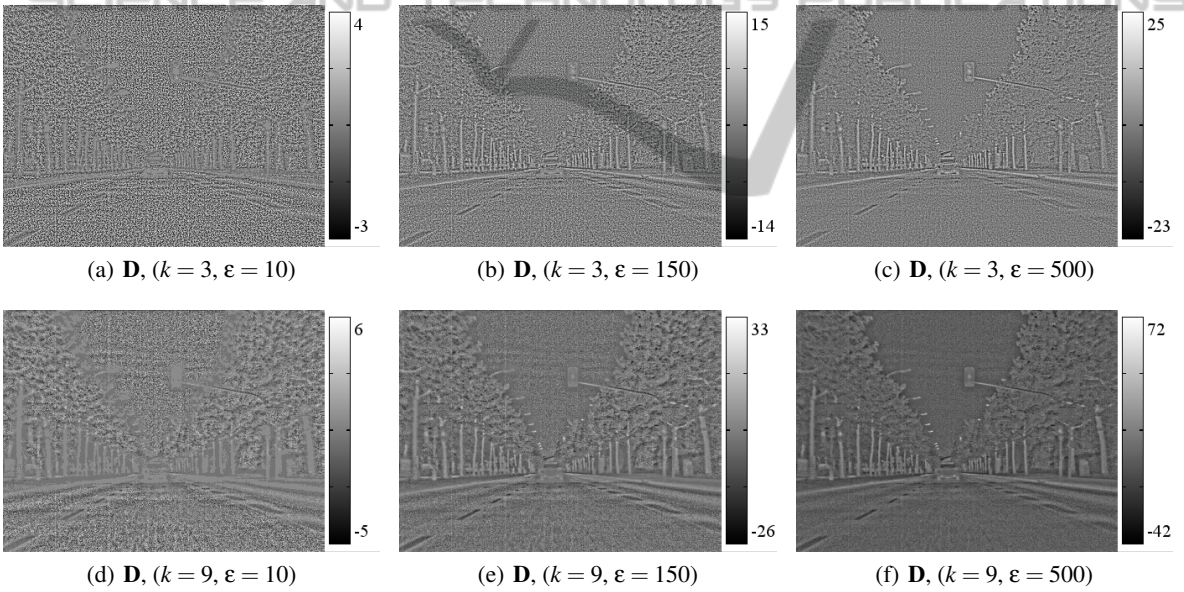

(a) **D**, ($k = 3$, $\varepsilon = 10$) (b) **D**, ($k = 3$, $\varepsilon = 150$) (c) **D**, ($k = 3$, $\varepsilon = 500$)

(d) **D**, ($k = 9$, $\varepsilon = 10$) (e) **D**, ($k = 9$, $\varepsilon = 150$) (f) **D**, ($k = 9$, $\varepsilon = 500$)

Figure 4: Resulting detail image **D** depending on the filter parameters.

reduce the amount of noise by masking **D** using $\bar{\mathbf{a}}_i$, *i.e.,* $\mathbf{D}' = \lambda\bar{\mathbf{a}}_i \cdot \mathbf{D}$, with λ a gain factor to increase, if desired, the contrast of the details in **D**. We present, in Fig. 5, the enhanced $\mathbf{D}'$ image component after being masked using $\bar{\mathbf{a}}_i$. In addition, we also illustrate the behaviour of increasing the λ gain.

3.3 8 bit Data Representation

In general, DDE filters based on raw image splitting compress the HDR of **B** using extended histogram equalization techniques for its conversion to the 8 bit domain. The final 8 bit enhanced image **O** results from the sum of the compressed **B** and the enhanced $\mathbf{D}'$, *i.e.,* $\mathbf{O} = \mathbf{B} + \mathbf{D}'$ (Durand and Dorsey, 2002; Liu and Zhao, 2014; Zuo et al., 2011). However, this straightforward combination of **B** and $\mathbf{D}'$ yields to saturation in most of the cases since pixel values of $\mathbf{D}'$ are considerable if compared to the 8 bit data range representation, *e.g.,* see the data range representation

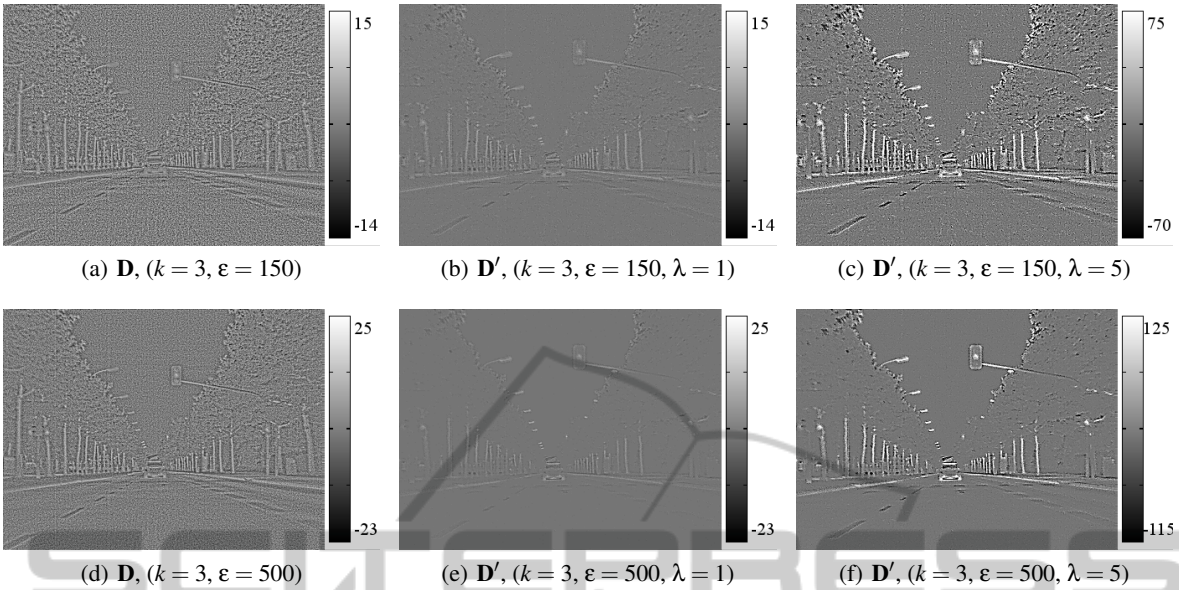

(a) $\mathbf{D}$, ($k = 3, \varepsilon = 150$) (b) $\mathbf{D}'$, ($k = 3, \varepsilon = 150, \lambda = 1$) (c) $\mathbf{D}'$, ($k = 3, \varepsilon = 150, \lambda = 5$)

(d) $\mathbf{D}$, ($k = 3, \varepsilon = 500$) (e) $\mathbf{D}'$, ($k = 3, \varepsilon = 500, \lambda = 1$) (f) $\mathbf{D}'$, ($k = 3, \varepsilon = 500, \lambda = 5$)

Figure 5: Resulting detail image $\mathbf{D}'$ after noise masking and detail magnification.

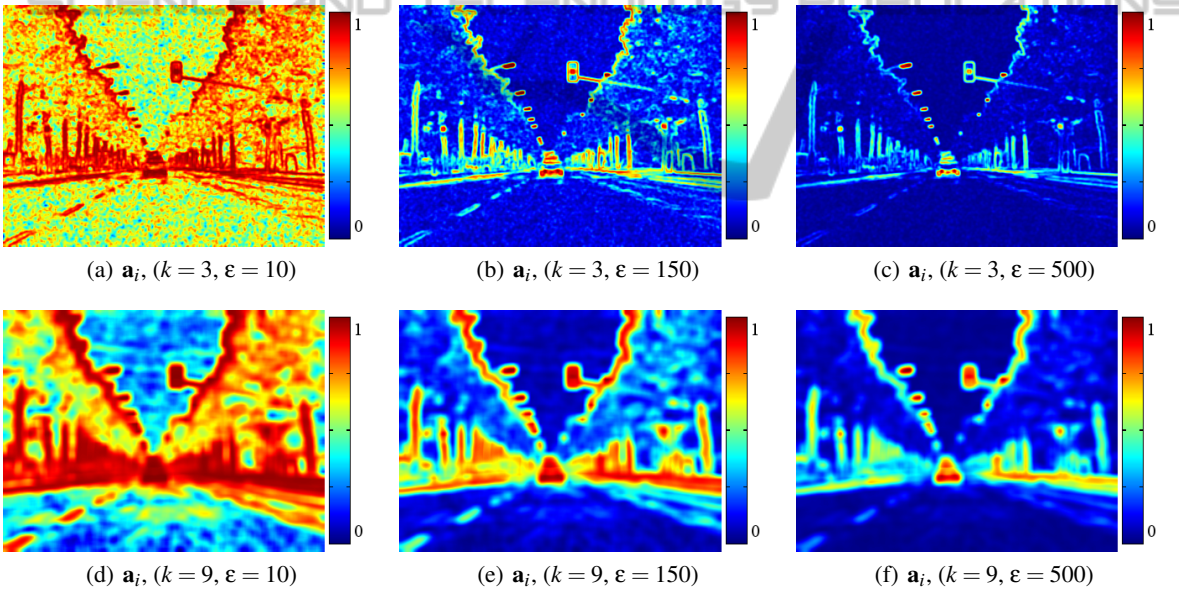

(a) $\mathbf{a}_i$, ($k = 3, \varepsilon = 10$) (b) $\mathbf{a}_i$, ($k = 3, \varepsilon = 150$) (c) $\mathbf{a}_i$, ($k = 3, \varepsilon = 500$)

(d) $\mathbf{a}_i$, ($k = 9, \varepsilon = 10$) (e) $\mathbf{a}_i$, ($k = 9, \varepsilon = 150$) (f) $\mathbf{a}_i$, ($k = 9, \varepsilon = 500$)

Figure 6: Resulting $\mathbf{a}_i$ depending on the filter parameters.

in Fig. 5(f).

Following the TDDE filter diagram flow presented in Fig. 1, we combine both $\mathbf{B}$ and $\mathbf{D}'$ image components before being converted to 8 bit data representation. By doing so, we avoid the data rearrangement process which might require manual tuning depending on the filter and gain factor parameters (Liu and Zhao, 2014; Zuo et al., 2011).

To address the 8 bit data conversion, we have adopted the LAGC approach presented in (Liu et al., 2012). According to (Liu et al., 2012), LAGC incorporates human visual properties in their design of the detail enhancement. Indeed, LAGC is based on the Weber's law, which is commonly used in cases where fine details are present on a large uniform background. As a result, details that can be hardly seen on darker and/or brighter background become perceptible by the human eye.

In practice, the active data range in the raw IR image $\mathbf{I}$ is generally narrow and thus, a linear extension

of the active range will ensure a significant variation of the background intensity, *i.e.,*

$$\mathbf{I}''(i,j) = \frac{(2^M-1)(\mathbf{I}'(i,j) - I^t_{min})}{I^t_{max} - I^t_{min}}, \quad (4)$$

with $\mathbf{I}' = \mathbf{B} + \mathbf{D}'$, M the number of bits (12 or 14) to encode $\mathbf{I}$, and I^t_{min} and I^t_{max} the limits of the active data range computed from a temporal statistical stabilization, *i.e.,*

$$I^t_{max} = \bar{\mu}_t + k_1\bar{\sigma}_t \quad (5)$$
$$I^t_{min} = \bar{\mu}_t - k_2\bar{\sigma}_t, \quad (6)$$

with k_1 and k_2 defining the active data range to be considered in the 8 bit representation. From our experiments, $k_1 = 3$ and $k_2 = 1$ provide good results to enhance the perception of warm objects.

$$\bar{\mu}_t = \alpha \cdot \mu_t + (1-\alpha)\cdot\bar{\mu}_{t-1} \quad (7)$$
$$\bar{\sigma}_t = \alpha \cdot \sigma_t + (1-\alpha)\cdot\bar{\sigma}_{t-1}, \quad (8)$$

are respectively the adapted mean and standard deviation of $\mathbf{I}$ at time t, with μ_t and σ_t the respective mean and standard deviation of $\mathbf{I}$ at time t ($\bar{\mu}_0 = \mu_0 = 0$ and $\bar{\sigma}_0 = \sigma_0 = 0$). $\alpha \in [0,1]$ defines the speed to adapt I^t_{min} and I^t_{max} to the limits of the active data range of frame t. Thereby, the smaller the α value, the smoother the global brightness fluctuations between frames.

The human eye can hardly distinguish small brightness differences such as image details on dark or bright backgrounds. In contrast, the same brightness differences become perceptible in the middle backgrounds. This behaviour is modelled by the Weber's law and it has been used to design the local adaptive gamma value as follows

$$\gamma(i,j) = \max\Big(\exp\Big(\frac{\mathbf{B}(i,j) - 2^{M-1}}{2^{M-1}}\Big), 1\Big), \quad (9)$$

where we consider the $\mathbf{B}$ image component as a mild background representation. From (9), brightness differences are significantly magnified for $\mathbf{B}$ values greater than 2^{M-1} which meets the purpose of the Weber's law to enhance warmer objects. That is, LAGC must be only applied when $\gamma \geq 1$. The final 8 bit image representation results from

$$\mathbf{O}(i,j) = (2^N - 1)\cdot\Big(\frac{\mathbf{I}''(i,j)}{2^M-1}\Big)^{\gamma(i,j)}, \quad (10)$$

with $N = 8$ for data representation within the range $[0,255]$.

4 EXPERIMENTAL EVALUATION

In the following, we evaluate the presented TDDE filter using real scenes acquired by a prototype thermal camera that provides HDR IR images of (384 × 288) pixels. All reported results have been obtained using an Intel® Core™ i5-4200U CPU @ 1.60GHz with an integrated graphic card Intel® HD Graphics 4400.

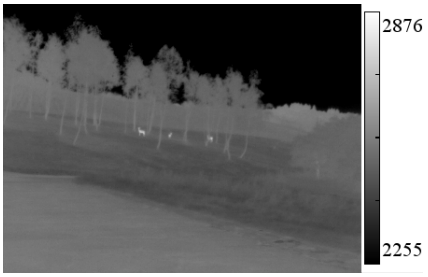

(a)

(b)

Figure 7: Considered night vision scenes for evaluation. (a) Forest scene. (b) City scene.

The proposed TDDE filter has been compared against the most recent DDE-based techniques, *i.e.,* BF&DDE and GF&DDE. All DDE-based approaches have been implemented in C++ language using the OpenCV (Bradski and Kaehler, 2008) library.

Fig. 8 presents and compares the resulting 8 bit image after applying BF&DDE, GF&DDE, and the proposed TDDE filter on two real night vision scenes, *i.e.,* forest and city scene (see Fig. 7). The forest scene presents very fine details such as trees' leaves, and a group of deer that is almost non-perceptible in the raw IR image. The city scene is a more challenging case due to the high variability of temperature ranges, *e.g.,* sky, cars and people.

Although BF&DDE and GF&DDE present very close results, we can appreciate more satisfactory results when applying the TDDE filter. Indeed, warm objects can be better perceived from the background as a consequence of the dedicated LAGC implementation to handle warm pixels (see Section 3.3). In addition, it avoids undesirable artefacts such as the amplification of the noise within the sky and fine details become perceptible to the human eye, *e.g.,* deer and trees' leaves (in the forest scene), or people and car edges (in the city scene) are better enhanced, presenting an improvement on the global sharpness of the

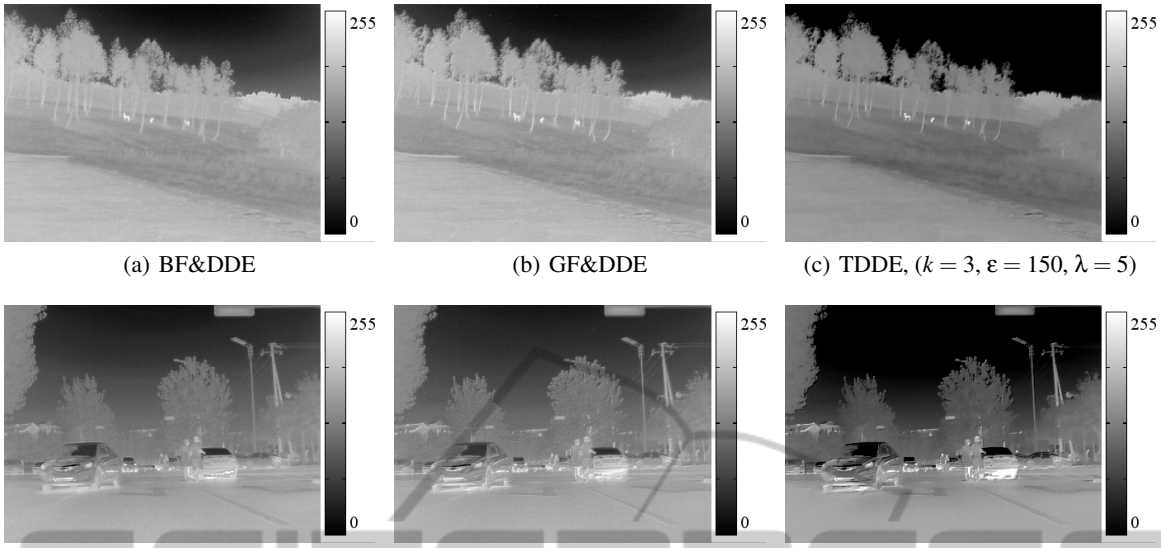

(a) BF&DDE (b) GF&DDE (c) TDDE, ($k = 3$, $\varepsilon = 150$, $\lambda = 5$)

(d) BF&DDE (e) GF&DDE (f) TDDE, ($k = 3$, $\varepsilon = 150$, $\lambda = 5$)

Figure 8: Comparison between BF&DDE, GF&DDE, and the proposed TDDE filter. 1^{st} row. Forest scene with almost non-perceptible details (trees' leaves and deers). 2^{nd} row. City scene with high variability of temperature ranges (sky, cars and people).

image.

We have considered the EMEE contrast metric, or the measure of enhancement by entropy (Agaian et al., 2001) to quantify the contrast improvement when using BF&DDE, GF&DDE, or the proposed TDDE filter. The EMEE metric has proven to provide a contrast measurement that is well adapted to the human subjective analysis. This metric is also defined from the Weber's law, used in the design of γ in eq. (9). Table 1 reports the result of the EMEE on the scenes presented in Fig. 8. Although the TDDE filter performs better in all cases, a subjective evaluation might be needed to appreciate the improvement of the TDDE filter compared to BF&DDE and/or GF&DDE. We hence invite the reader to watch the attached comparative videos. From these videos, it is also noticeable how the proposed TDDE filter avoids global brightness fluctuations from frame to frame as a result of limiting the active data range, using temporal statistical stabilization, when mapping the raw IR image to 8 bit domain. To evaluate the global brightness stabilization along time, we have considered the scene presented in Fig. 9 where a pedestrian crosses the street through the field-of-view of the camera. The pedestrian is a large bright object entering suddenly into the field-of-view of the camera, which induces to a rapid change of the histogram distribution. In Fig. 10 the time evolution of the mean of the resulting **O** after applying the TDDE filter is compared with the one resulting from BF&DDE and GF&DDE. As can be observed, TDDE provides a smoother change of the global brightness as well as a significantly smoothed variation along time. However, the pedestrian is close to the saturation limit as a result of preserving the global brightness level close to the previous frame. This behaviour can be further adjusted by tuning the α parameter in eq. (8).

Table 1: Evaluation of BF&DDE, GF&DDE, and the proposed TDDE filter using the EMEE contrast metric.

	BF&DDE	GF&DDE	TDDE
Forest scene (1^{st} row of Fig. 8)	0.227	0.312	0.377
City scene (2^{nd} row of Fig. 8)	0.219	0.216	0.554

Table 2 reports the performance evaluation of BF&DDE, GF&DDE and the proposed TDDE filter. As can be observed in the table, the TDDE filter performs much faster than BF&DDE and/or GF&DDE, which makes it a very promising choice for real world applications.

Table 2: Running time detail to compute the 8 bit representation of the raw **I** shown in Fig. 2 (units are in ms).

Algorithm	**B**	**D**	**O**	Total
BF&DDE	55.26	6.63	4.06	65.95
GF&DDE	4.33	1.95	4.05	10.33
TDDE	4.28	0.47	10.54	15.55

(a) BF&DDE, ($t = 0$) (b) BF&DDE, ($t = 160$) (c) BF&DDE, ($t = 226$)

(d) GF&DDE, ($t = 0$) (e) GF&DDE, ($t = 160$) (f) GF&DDE, ($t = 226$)

(g) TDDE, ($t = 0$) (h) TDDE, ($t = 160$) (i) TDDE, ($t = 226$)

Figure 9: Comparison of global brightness temporal stability of DDE-based contrast enhancement methods.

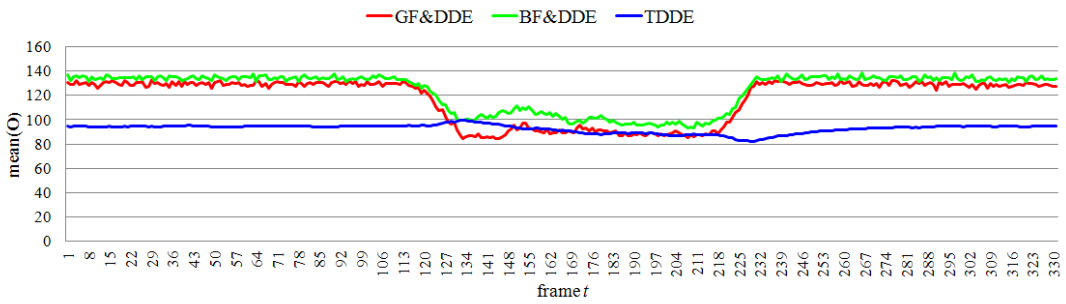

Figure 10: Comparison of temporal stability of the histogram mean for BF&DDE, GF&DDE and TDDE.

5 CONCLUSIONS

A new detail enhancement technique for visualization of HDR IR images has been presented. Similarly to the most recent DDE-based filters, *i.e.,* BF&DRP (Branchitta et al., 2009), BF&DDE (Zuo et al., 2011), and GF&DDE (Liu and Zhao, 2014), the proposed TDDE filter also splits the raw IR image into base and detail image components. This in turn enables for an independent and dedicated processing to compress the HDR while enhancing quasi non-perceptible image details. GF has been considered to split the raw IR image. Indeed, in addition to significantly reduce the amount of noise within the resulting base image component, it presents a better behaviour near edges (compared to BF) with a major advantage of being suitable for real-time applications. Furthermore, the linear coefficients of the GF reflect the spa-

tial detail of the raw IR, allowing us to identify those regions that are prominent to present noise. Therefore, noise removal is addressed by masking the detail image component with the GF linear coefficients. We note that the fact of treating the detail image according to the likelihood to present noise enables to reduce the ε parameter of the GF and thus to preserve finer details. Both base and detail image components have been combined and converted to the 8 bit domain using a local adaptive gamma correction that has been designed based on the Weber's law. By doing so, non-perceptible details in front of dark or bright backgrounds are magnified to become perceptible by the human eye in the resulting 8 bit image. It is in this last stage where we have limited the active HDR range computed through time in order to avoid global brightness fluctuations from frame to frame. From the experiments, we show that the TDDE filter effectively addresses the compression of the HDR with a human vision based enhancement of the image details. Noise within uniform regions is almost suppressed and its efficiency makes it a practical approach for real world applications such as night vision for driver assistance system or surveillance in security. As a future work, we would like to investigate the possibility of combining two dedicated GF to split the raw IR image in order to better address noise removal and detail enhancement.

REFERENCES

Agaian, S., Panetta, K., and Grigoryan, A. (2001). Transform based image enhancement with performance measure. In *IEEE Transactions on Image Processing*, pages 367–381.

Bradski, G. and Kaehler, A. (2008). *Learning OpenCV: Computer Vision with the OpenCV Library*. O'Reilly Media, 1st edition.

Branchitta, F., Diani, M., Corsini, G., and Porta, A. (2008). Dynamic-range compression and contrast enhancement in infrared imaging systems. *Optical Engineering*, 47(7):076401:1–14.

Branchitta, F., Diani, M., Corsini, G., and Romagnoli, M. (2009). New technique for the visualization of high dynamic range infrared images. *Optical Engineering*, 48(9):096401:1–9.

Durand, F. and Dorsey, J. (2002). Fast Bilateral Filtering for the Display of High-Dynamic-Range Images. *ACM Trans. Graph.*, 21(3):257–266.

Glushko, S. W. and Salvaggio, C. (2007). Quantitative analysis of infrared contrast enhancement algorithms. In *Infrared Imaging Systems: Design, Analysis, Modeling, and Testing*, pages 65430S:1–12.

He, K., Sun, J., and Tang, X. (2013). Guided Image Filtering. *IEEE Transactions on Pattern Analysis and Machine Intelligence*, 35(6):1397–1409.

Karali, A. O., Okman, O. E., and Aytac, T. (2010). Adaptive enhancement of infrared images containing sea surface targets. In *IEEE Signal Processing and Communications Applications Conference (SIU)*, pages 605–608.

Kim, J. Y., Kim, L. S., and Hwang, S. H. (2001). An advanced contrast enhancement using partially overlapped sub-block histogram equalization. *IEEE Transactions on Circuits and Systems for Video Technology*, 11(4):475–484.

Liang, K., Ma, Y., Xie, Y., Zhou, B., and Wang, R. (2012). A new adaptive contrast enhancement algorithm for infrared images based on double plateaus histogram equalization. *Infrared Physics and Technology*, 55(4):309–315.

Liu, B., Wang, X., Jin, S., Chen, Y., Liu, C., and Liu, X. (2012). Infrared image detail enhancement based on local adaptive gamma correction. *Chinese Optics Letters*, 10(2):021002:1–5.

Liu, N. and Zhao, D. (2014). Detail enhancement for high-dynamic-range infrared images based on guided image filter. *Infrared Physics and Technology*, 67:138–147.

Pizer, S. M., Amburn, E. P., Austin, J. D., Cromartie, R., Geselowitz, A., Greer, T., Romeny, B. T. H., and Zimmerman, J. B. (1987). Adaptive Histogram Equalization and its Variations. *Comput. Vision Graph. Image Process.*, 39(3):355–368.

Silverman, J. (1993). Signal-processing algorithms for display and enhancement of ir images. In *Infrared Technology*, pages 440–450.

Vickers, V. E. (1996). Plateau equalization algorithm for realtime display of highquality infrared imagery. *Optical Engineering*, 35(7):1921–1926.

Zuiderveld, K. (1994). Graphics gems iv. In Heckbert, P. S., editor, *Image Processing*, chapter Contrast Limited Adaptive Histogram Equalization, pages 474–485. Academic Press Professional, Inc.

Zuo, C., Chen, Q., Liu, N., Ren, J., and Sui, X. (2011). Display and detail enhancement for high-dynamic-range infrared images. *Optical Engineering*, 50(12):127401:1–9.